First-passage-time distribution in a moving parabolic potential with spatial roughness

Yongge Li,[1] Yong Xu,[2,3,*] and Jürgen Kurths[4,5]

[1]*Center for Mathematical Sciences & School of Mathematics and Statistics, Huazhong University of Science and Technology, Wuhan 430074, China*

[2]*Department of Applied Mathematics, Northwestern Polytechnical University, Xi'an 710072, China*

[3]*MIIT Key Laboratory of Dynamics and Control of Complex Systems, Northwestern Polytechnical University, Xi'an 710072, China*

[4]*Potsdam Institute for Climate Impact Research, Potsdam 14412, Germany*

[5]*Human and Animal Physiology Department, Saratov State University, Saratov 410000, Russia*

(Received 14 January 2019; published 3 May 2019)

In this paper, we investigate the first-passage-time distribution (FPTD) within a time-dependent parabolic potential in the presence of roughness with two methods: the Kramers theory and a nonsingular integral equation. By spatially averaging, the rough potential is equivalent to the combination of an effective smooth potential and an effective diffusion coefficient. Based on the Kramers theory, we first obtain Kramers approximations (KAs) of FPTD for both smooth and rough potentials. As expected, KA is valid only for high barriers and small external forces, and generally applicable for high barriers in rough potentials. To overcome the shortcoming of KA, a probability asymptotic approximation (PAA) based on an integral equation is proposed, which uses the transient probability density function (PDF) of the natural boundary conditions instead of the absorbing boundary conditions. We find that PAA fits very well even for large external forces. This enables us to analytically solve the FPTD for large external forces and low barriers as a strong extension to KA. In addition, we show that in the presence of a rough potential, the PAA of FPTD is in good agreement with numerical simulations for low barrier potentials. The PAA makes it possible to investigate the first-passage problem with ultrafast varying potentials and short exiting time. Thus, KA and PAA are complementary in determining the FPTD both for various barriers and external forces. Finally, the mean first-passage time (MFPT) is studied, which illustrates that the PAA of MFPT is effective almost in the whole range of external forces, while the KA of MFPT is valid only for small external forces.

DOI: 10.1103/PhysRevE.99.052203

I. INTRODUCTION

The first-passage problem describes that a system escapes from a certain area for the first time to other states. This problem has found applications in various fields, such as critical transitions in ecosystems, climate, structural reliability, target searching, financial market, and protein dynamics [1–6]. First-passage-time distribution (FPTD), mean first-passage time (MFPT), and transition paths are typically used to quantify and measure such first-passage processes in different systems [6–11]. Mathematically, these terms can be derived directly or indirectly from transient probability density functions (PDFs) by solving the corresponding Fokker-Planck equation (FPE) with absorbing boundary conditions [10,11]. However, it is generally difficult to derive the transient PDF for such boundary conditions, even for the very simple parabolic potential cases [10–12]. This is why there are surprisingly few analytical results of FPTD. Thus, different methods and theories have been developed to approximate FPTD, such as the Kramers escape theory, the path integral method, and weak noise limit theory [13–27].

The Kramers theory is one of the most popular methods to solve the MFPT, transition rate, and net flux on theoretical approaches and applications to experimental systems. Hänggi *et al.* [14] and Mel'nikov [15] have presented a detailed development of the Kramers theory including applications in their reviews. Recently, it was applied to analyze bond rupture in molecule pulling experiments, where the FPTD and the mean of the rupture force are obtained [16–20]. However, due to the high barrier assumption of the Kramers theory, a good fitting between analytical results and experimental data has only been found for slow pulling speeds, which restricts the analysis of fast pulling speeds and large external forces. Moreover, the path integral method, a powerful semianalytical and seminumerical method, can also be used to estimate the FPTD for different kinds of noises, such as Gaussian noise and Lévy noise [21,22]. Despite its high accuracy, it is not explicit and intuitive to evaluate the influences of different factors directly. This is also the shortcoming of the integral equation, which sets up a relationship between FPTD and PDFs under natural and absorbing boundary conditions. For this method, explicit results are limited to simple potentials when the absorbing boundary locates at the bottom of the potentials, such as linear and parabolic potentials [13]. Recently, Bullerjahn *et al.* took a further step based on the integral equation and got a first-order approximation of the net flux, and applied this to the analysis of rapid force spectroscopy [23]. They found that this approximation could fit well for large external forces and fast pulling rates which is quite different from the Kramers results. Besides, there is another form of a nonsingular integral equation given by Buonocore *et al.* establishing a relationship

*hsux3@nwpu.edu.cn

between FPTD and PDF under natural boundary conditions by two unknown functions to be determined [24]. Based on this relationship, Giorno provided a way to determine the unknown functions resulting in a simple equation [25]. In this paper, we take advantage of this method, and extend it to a moving parabolic potential with roughness.

Rough potential is universal in various systems, such as structural glasses, ion channel, supercooled liquid, and especially in protein or molecular dynamics [28–35]. Compared to classic smooth potentials, rough potential has not yet been widely and deeply investigated either theoretically or numerically, despite its enormous practical applications. Zwanzig modeled the roughness by superimposing a fast changing trigonometric function to the background potential, and stated a conjecture which is applicable for specific cases [36]. Pollak *et al.* studied the rate theory for rugged energy landscapes with a master equation [37], while Ansari directly used a robust numerical approach to solve the Smoluchowski equation in the presence of roughness [38]. Mondal *et al.* found that roughness slowed down the current in a ratchet potential subject to Gaussian noise [39]. However, under Lévy noise, we have shown recently that roughness could accelerate the barrier crossing process and increase the current [40–42]. This phenomenon indicates that roughness has diverse influences on the transport of particles, which can be either positive or negative. Thus, it is essential to analyze how roughness affects the barrier crossing process.

In this paper, we intend to investigate the FPTD in a rough parabolic potential with external forces. By superimposing a fast varying trigonometric function on the parabolic potential, we introduce the rough model and give a brief analysis of the first-passage problem in Sec. II. Two approximations of the FPTD are presented with detailed procedures via the Kramers theory and Giorno's equation, respectively, in Sec. III. Numerical results are calculated to verify the validity of both approximations, and discussions of their valid areas are provided in Sec. IV. Besides, two approximations of MFPTs are obtained for small external forces in Sec. V. Conclusions are given in Sec. VI.

II. MODEL DESCRIPTION AND FPTD

A. Model description

We consider the first-passage problem in a time-dependent parabolic potential. In a molecule rupture experiment, the first-passage problem can be seen as the break of polymer chains under moving pulling forces. Due to the complex and irregular structure of polymer chains, their energy potential surfaces are reasonably regarded as rough or rugged, so in this paper, we superimpose a rough factor, modeled by a fast changing trigonometric function from Zwanzig, on the classic smooth parabolic potential to obtain a rough potential. The corresponding Langevin equation of the model can be written as

$$\dot{x} = -\frac{D}{k_b T}\frac{\partial}{\partial x}U(x,t) + \sqrt{2D}\eta(t), \tag{1}$$

where the overdot above the variable x means the derivative of time. D is the diffusion coefficient. k_b and T are the Boltzmann's constant and temperature, respectively. For simplicity, we assume $k_bT = 1.0$. $\eta(t)$ is the standard Gaussian white noise. $U(x,t)$ is a time-dependent parabolic potential with rough factor, satisfying

$$U(x,t) = U_0(x) + U_1(x) + F(x,t), \quad U_0(x) = \frac{\Delta}{x_b^2}x^2,$$
$$U_1(x) = \varepsilon\cos(\omega x), \quad F(x,t) = -F_0 x t. \tag{2}$$

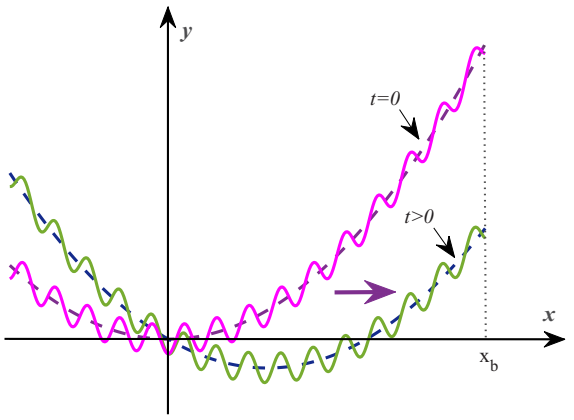

FIG. 1. Sketch of a time-dependent parabolic potential with rough surface. The solid lines are rough potentials, and the dashed lines are smooth parabolic potentials. With time going on, the potential moves to the right.

$U(x,t)$ consists of three parts: the basic parabolic potential $U_0(x)$, the rough part $U_1(x)$, and the time-dependent part $F(x,t)$. The absorbing boundary locates at $x = x_b$. Δ is the barrier height of the potential $U_0(x)$ at x_b. In the presence of an external force, the parabolic potential $U_0(x) + F(x,t)$ will change with time, and the bottom $\frac{x_b^2}{2\Delta}F_0 t$ moves to the right direction with the speed $\frac{x_b^2}{2\Delta}F_0$ as shown in Fig. 1. In the absence of noise excitations and roughness, the system can immediately adjust its position and mainly stays at the equilibrium point with a slowly varying external force. Hence, it will take about $\frac{2\Delta}{x_b F_0}$ time to exit the boundary x_b. This is the influence of external forces. In the presence of thermal fluctuations, influences of noises on the passage time are non-negligible. As expected, we show that the contributions to the MFPT come from two parts: the external force and thermal noise, respectively. This result is stated in Eq. (39) in Sec. V. $U_1(x)$ is to model the rough potential surface, in which ε is the amplitude of roughness, and ω is assumed to be a large number to ensure that $U_1(x)$ is a fast changing function. ω can control the density of the roughness, such that for a small ω the potential is a multistable potential rather than a rough one. To make sure that roughness acts as perturbations, $\varepsilon/\Delta \ll 1$ is assumed.

B. Analysis of FPTD

The first-passage can be described as the evolution of a particle initially starting from x_0, and passing over the boundary $x = x_b$ at some time t. This process corresponds to the FPE with an absorbing boundary at x_b, whose solution $p_a(x,t)$ satisfies $p_a(x > x_b, t|x_0, 0) = 0$, which means that the PDF is zero if a particle passes over the boundary $x = x_b$. The

FPE of Eq. (1) can be written as

$$\frac{\partial}{\partial t}p_a(x,t) = -\frac{\partial}{\partial x}[A(x,t)p_a(x,t)] + D\frac{\partial^2}{\partial x^2}p_a(x,t),$$
$$A(x,t) = -D\frac{\partial}{\partial x}U(x,t), \tag{3}$$

for which the initial and boundary conditions are set as

$$p_a(x,0) = \delta(x - x_0),$$
$$p_a(x_b,t) = p_a(-\infty,t) = 0. \tag{4}$$

Then the survival probability that a particle does not pass over $x = x_b$ at time t can be generated by a spatial integral on $p_a(x,t)$ as

$$S(t) = \int_{-\infty}^{x_b} p_a(x,t)dx. \tag{5}$$

Then the escape probability is $1 - S(t)$, whose derivative of time is the FPTD; i.e.,

$$f(x_b,t) = -\dot{S}(t). \tag{6}$$

Thus, $f(x_b,t)dt = -dS(t)$ is the probability that a particle passes over x_b for the first time in the interval $(t, t+dt)$. Here we denote $k(t)$ as the escape rate at time t. Consequentially, $S(t)k(t)$ is the current flowing across x_b, that is,

$$J_a(x_b,t) = S(t)k(t), \tag{7}$$

where $J_a(x_b,t) = A(x,t)p_a(x_b,t) - D\frac{\partial}{\partial x}p_a(x,t)|_{x=x_b}$. Combining Eqs. (5) and (6), one gets

$$\dot{S}(t) = \int_{-\infty}^{x_b}\frac{\partial}{\partial t}p_a(x,t)dx = -J_a(x_b,t). \tag{8}$$

In fact, the escape of particles only happens at the absorbing boundary $x = x_b$, which means the outflow $J_a(x_b,t)$ of particles is equal to changes of the survival probability $-\dot{S}(t)$. Following Eqs. (7) and (8), we know

$$\dot{S}(t) + S(t)k(t) = 0, \quad S(0) = 1. \tag{9}$$

The survival probability can be obtained by solving Eq. (9),

$$S(t) = \exp\left[-\int_0^t k(\tau)d\tau\right], \tag{10}$$

and the corresponding FPTD is

$$f(x_b,t) = k(t)\exp\left[-\int_0^t k(\tau)d\tau\right]. \tag{11}$$

Thus, the key to get the FPTD is to determine the escape rate $k(t)$. Otherwise, one should approximate $f(x_b,t)$ directly. Next, we will use two methods to approximate $k(t)$ and $f(x_b,t)$ respectively.

III. APPROXIMATIONS OF FPTD

In this section, we use two methods to get the FPTD. Firstly, we apply the Kramers theory to yield the escape rate $k(t)$ in the presence of external forces and roughness, and then obtain the FPTD with Eq. (11). Secondly, we try to approximate the FPTD directly with a transient PDF. However, it is generally very difficult to get the transient solution of Eq. (3) with absorbing boundary conditions. Instead, it is relatively easier to handle FPE with natural boundary conditions. Thus, we approximate the FPTD with a transient PDF of FPE with natural boundary conditions by solving an integral equation.

A. Kramers approximation

As known, the escape rate can be obtained by solving the Kramers problem, which is equal to the inverse of the MFPT. So in the case of a free-energy potential surface $U_0(x)$, the escape rate is a constant, which is given as

$$k_0^{-1} = \frac{1}{D}\int_b e^{U_0(x)}dx\int_{\text{well}} e^{-U_0(y)}dy. \tag{12}$$

To simplify the calculation of k_0 and avoid an overflow of the numerical simulation for the exponential part, we approximate the escape rate by an algebraic formula:

$$k_0 = N_1\frac{1}{\sqrt{\pi}}\frac{D\Delta^{1.5}}{x_b^2}e^{-\Delta}, \tag{13}$$

where N_1 is a coefficient to modulate the approximation (see details in the Appendix) [13]. We take $N_1 = 1.5$ in this paper. When we consider a practical system, such as the single-molecule rupture experiment, an external pulling force on the polymer chain should be added. In this case, the energy potential moves with time. For such a time-dependent potential, Hummer and Szabo [17] gave the corresponding escape rate as

$$k_F^{-1}(t) = \frac{1}{D}\int_{\text{b}} e^{[U_0(x)+F(x,t)]}dx\int_{\text{well}} e^{-[U_0(y)+F(y,t)]}dy. \tag{14}$$

The result can be written in an algebraic form:

$$k_F(t) = N_1\frac{1}{\sqrt{\pi}}\frac{D\Delta^{1.5}}{x_b^2}[1 - x_bFt/2\Delta]e^{-\Delta(1-x_bFt/2\Delta)^2}. \tag{15}$$

Substituting Eq. (15) into Eq. (11), one gets the FPTD

$$f_F(x_b,t) = k_0\left(1 - \frac{x_bFt}{2\Delta}\right)\exp\left\{\Delta - \Delta\left(1 - \frac{x_bFt}{2\Delta}\right)^2 - \frac{k_0}{x_bF}e^{\Delta[1-(1-\frac{x_bFt}{2\Delta})^2]}\right\}. \tag{16}$$

In the presence of roughness, the explicit expression of Eq. (14) is even complex and hard. In principle, we could solve it numerically to get the escape rate. However, it will not be intuitive to show the influences of roughness. To highlight the effects of roughness, we adopt the spatial averaging from Zwanzig's paper [36]. Because the rough part is assumed to be a small disturbance on the background potential, the integral can be approximated by

$$\int e^{U_0(x)+F(x,t)+U_1(x)}dx \cong \int e^{U_0(x)+F(x,t)}\langle e^{U_1(x)}\rangle dx, \tag{17}$$

in which $\langle\cdots\rangle$ is the spatial average over a length scale Δx. When $U_1(x) = \varepsilon\cos(\omega x)$ and $\Delta x = \pi/\omega$, the spatial averaging $\langle e^{U_1(x)}\rangle$ reduces to a modified Bessel function taking the form $\langle e^{U_1(x)}\rangle = \pi^{-1}\int_0^\pi e^{\varepsilon\cos x}dx$. Therefore we see $\langle e^{U_1(x)}\rangle = \langle e^{-U_1(x)}\rangle = I_0(\varepsilon)$, which is a function of ε independent of x.

Thus, the escape rate in the rough case takes the form

$$k_R^{-1}(t) = \frac{1}{D^*}\int_b e^{U^*(x,t)}dx \int_{\text{well}} e^{-U^*(y,t)}dy, \tag{18}$$

where $U^*(x,t) = U_0(x) + F(x,t) + \ln[I_0(\varepsilon)]$ is the effective potential, and $D^* = D/I_0^2(\varepsilon)$ is the effective diffusion coefficient. Therefore Eq. (18) is simplified to

$$k_R(t) = I_0^{-2}(\varepsilon)k_F(t). \tag{19}$$

Accordingly, we could get the FPTD under the rough potential $f_R(x_b,t)$.

B. Probability asymptotic approximation

The FPTD depends highly on the time evolution of the transient PDF. Thus the quasistationary and high barrier assumptions of the Kramers theory will probably make KA lose its effectiveness for low barriers and fast changing potentials. To overcome this shortcoming, basing on a nonsingular integral equation [24], we approximate the FPTD with the transient PDF of FPE with natural boundary conditions. This enables us to get a good approximation of FPTD applicable even to low barriers and fast changing potentials. From the results of Eq. (26), we see that the FPTD can be approximated by a transient PDF of natural boundary conditions via continuous iteration, so we here call this *probability asymptotic approximation*.

For convenience, to distinguish the PDF $p_a(x,t)$ of the absorbing boundary case, we denote $p_n(x,t)$ as the PDF of the natural boundary case; i.e., $p_n(x,t)|_{x\to\pm\infty} = 0$. Under natural boundary conditions, we note that particles at the point of $x = x_b$ come from two sources: One is the contribution from the domain $x < x_b$ which are real survival particles; the others are the backflow of particles from $x > x_b$ which passed over $x = x_b$ at some time $\tau < t$. This can be described by the following equation:

$$p_a(x,t) = p_n(x,t) - \int_0^t f(\tau)p_n(x,t|x_b,\tau)d\tau, \quad x \leqslant x_b. \tag{20}$$

This integral equation is widely used [13,23] to describe the first-passage problem. However, it is difficult to analytically get either two of $p_a(x,t)$, $f(t)$ and $p_n(x,t)$. So in this paper, we use another form of integral equation. Buonocore *et al.* gave such an integral equation for a time-independent drift [24],

$$f(x_b,t) = -2\varphi(x_b,t) + 2\int_0^t f(x_b,\tau)\varphi(x_b,t|x_b,\tau)d\tau, \tag{21}$$

in which $\varphi(x_b,t)$ takes the following form:

$$\varphi(x_b,t|z,\tau) = -J_n(x_b,t|z,\tau) + m(t)p_n(x_b,t|z,\tau) + r(t)[1 - S(x_b,t|z,\tau)]. \tag{22}$$

J_n and p_n are the probability flux and PDF under natural boundary conditions. $m(t)$ and $r(t)$ are two functions to be determined. Giorno *et al.* [25] gave a regime to handle this pair of unknown functions. They simplified the process by assuming $r(t) = 0$. Then $m(t)$ can be uniquely determined by the condition

$$\lim_{\tau\to t}\varphi(x_b,t|x_b,\tau) = 0. \tag{23}$$

The solution of $m(t)$ is given under the condition of a time-independent drift term; i.e., $m(t) = A(x)/2$. For a time-dependent drift, we find that this also holds; i.e.,

$$m(t) = \tfrac{1}{2}A(x,t). \tag{24}$$

Combining Eqs. (22) and (24) yields

$$\varphi(x_b,t) = -\frac{1}{2}A(x_b,t)p_n(x_b,t) + D\frac{\partial}{\partial x}p_n(x,t)\Big|_{x=x_b}. \tag{25}$$

Substituting Eq. (25) into Eq. (21), one obtains the formally solvable equation with one unknown factor $f(x_b,t)$. However, even so, Eq. (21) is an integral equation and it is difficult to solve. Alternatively, $f(x_b,t)$ can be explicitly generated by iterating Eq. (21), i.e.,

$$\begin{aligned} f(x_b,t) =& -2\varphi(x_b,t) - 4\int_0^t \varphi(x_b,t)\varphi(x_b,t|x_b,\tau_1)d\tau_1 - \cdots - (-2)^n\int_0^t\int_0^{\tau_1}\cdots\int_0^{\tau_{n-2}} \varphi(x_b,t|x_b,\tau_1)\cdots \\ & \varphi(x_b,\tau_{n-2}|x_b,\tau_{n-1})\varphi(x_b,\tau_{n-1})d\tau_{n-1}\cdots d\tau_1 - (-2)^{n+1}\int_0^t\int_0^{\tau_1}\cdots\int_0^{\tau_{n-1}} \varphi(x_b,t|x_b,\tau_1)\cdots \\ & \varphi(x_b,\tau_{n-1}|x_b,\tau_n)f(x_b,\tau_n)d\tau_n\cdots d\tau_1, \end{aligned} \tag{26}$$

where $0 < \tau_n < \tau_{n-1} < \ldots < \tau_1 < t$, and $f(x_b,\tau_n)$ will vanish for $n\to\infty$ and $\tau_n \to 0$. For simplicity, we take the first term of the right-hand side (rhs) of Eq. (26) as an approximation of $f(x_b,t)$; thus

$$f(x_b,t) \approx A(x_b,t)p_n(x_b,t) - 2D\frac{\partial}{\partial x}p_n(x,t)\Big|_{x=x_b}. \tag{27}$$

Next, the only term left is $p_n(x_b,t)$. In this part, we take a smooth potential as an example. Under natural boundary conditions, the corresponding FPE of Eq. (1) can be written as

$$\frac{\partial}{\partial t}p_n(x,t) = -\frac{\partial}{\partial x}[A(x,t)p_n(x,t)] + D\frac{\partial^2}{\partial x^2}p_n(x,t). \tag{28}$$

The transient PDF can then be solved analytically [23],

$$p_n(x,t) = \frac{1}{\sqrt{2\pi}\sigma}\exp\left\{-\frac{[x - \bar{x}(t) - x_0C_t]^2}{2\sigma^2}\right\}, \tag{29}$$

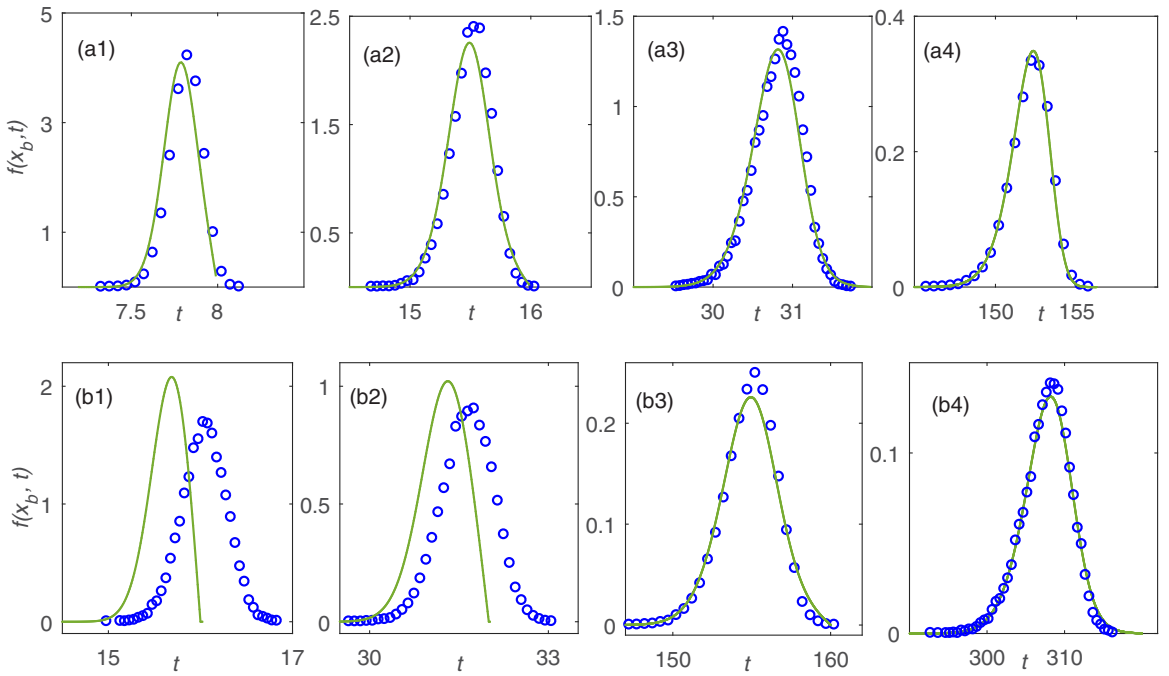

FIG. 2. Comparisons of KA of FPTD (solid lines) and numerical simulations (symbols) with respect to different F_0. (a) $D = 0.05$. From left to right, the solid lines and symbols correspond to $F_0 = 200,\ 100,\ 50,\ 10$; (b) $D = 0.005$. From left to right, the solid lines and symbols correspond to $F_0 = 100,\ 50,\ 10,\ 5$.

where $\bar{x}(t)$ is the mean position of particles taking the form

$$\bar{x}(t) = x_0 C_t + \frac{x_b^2}{2\Delta} F_0 t - \frac{x_b^4 F_0}{4D^*\Delta^2}(1 - C_t), \tag{30}$$

with

$$\sigma^2 = x_b^2\left(1 - C_t^2\right)/2\Delta, \quad C_t = e^{-2D\Delta t/x_b^2}. \tag{31}$$

Combining Eqs. (27) and (29)–(31), we get the explicit PAA of FPTD as

$$f(x_b, t) \approx D\left\{-\frac{2\Delta}{x_b} + F_0 t + \frac{2}{\sigma^2}[x_b - \bar{x}(t)]\right\} p_n(x_b, t). \tag{32}$$

Then the final $f(x_b, t)$ is obtained in the smooth potentials case. Accordingly, $f(x_b, t)$ in rough potentials can be derived by replacing D by D^*, and substituting $p_n(x_b, t)$ of the rough case in Eq. (32).

IV. SIMULATIONS AND DISCUSSIONS

In this part, we try to test and analyze the effectiveness of KA and PAA. Due to the superposition of a rough potential, when numerically simulating Eq. (1), the time step should be sufficiently small to evaluate the influences of roughness, so in this paper, the numerical time step is taken as 10^{-4}, and each curve in the following figures is averaged over 10^3 trajectories. Because when ω is small the phase of $U_1(x)$ directly affects the directions of the first proceeding step, the frequency ω in $U_1(x)$ should be large enough to eliminate the influence of the phases. Therefore we choose $\omega = 93$ in this paper. As shown in Eqs. (16) and (32), with time going on, $f(x_b, t)$ will change from positive to negative. Ensuring the non-negativity of probability, only the positive part of $f(x_b, t)$ is valid, so in the following figures, we only show the positive part with normalization except as otherwise noted.

A. Validity of KA

As is known, the Kramers theory is based on the high barrier limit to guarantee that the probability flux over the top of the barrier is sufficiently small. In Fig. 2, we choose a high barrier parameter $\Delta = 1600$ at $x_b = 2.0$. The diffusion constant is set as either $D = 0.05$ or $D = 0.005$ to illustrate its influences on the accuracy of the KA. The solid lines refer to KA [Eq. (16)], and the cycles are numerical results for smooth potentials. When $D = 0.05$ in Fig. 2(a), the analytical results and the numerical simulations are in better agreement for smaller F_0. For large F_0, although the fitting is not so good, the shapes of numerical and analytical FPTDs have some common ground, e.g., almost the same position of the maximum and a good agreement on the left tails. In this case, the analytical MFPT will probably have little difference with numerical results. However, in Fig. 2(b) when $D = 0.005$, the KA breaks down for large external forces. Comparing Figs. 2(a2)–2(a4) and 2(b1)–2b(3), we find that for fixed F_0, KA becomes relatively bad for smaller D. So both F_0 and D affect the effectiveness of KA. Next we discuss how they affect it.

In the presence of the external force, the original static potential starts to move with time. Thus, the barrier at the boundary x_b becomes lower and lower, and eventually vanishes when $t_c = 2\Delta/x_b F_0$, after which $k_F(t)$ will be negative. It can be seen in Fig. 2 that KA fails to match numerical results when the rhs tail of $f(x_b, t)$ has a nonzero derivative with respect to t. To explain this, we write the FPTD as $f(x_b, t) = k(t)S(t)$. It is clear that the nonzero derivative is caused by

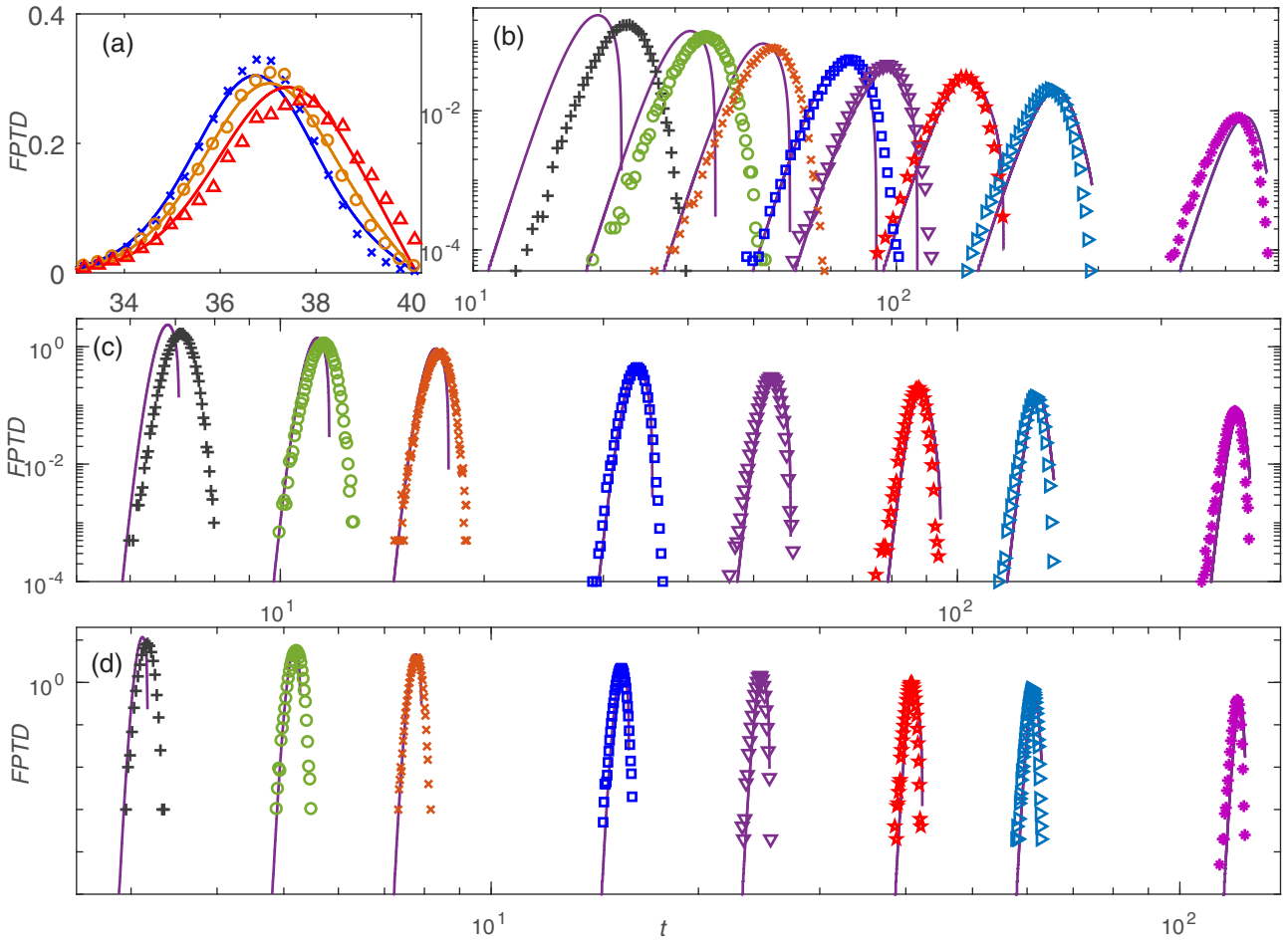

FIG. 3. Comparisons of KA and numerical simulations FPTDs in the presence of roughness, $D = 0.05$. (a)$\Delta = 200$, $N_1/N_2 = 0.5$; from left to right symbols and lines correspond to $\varepsilon = 0.5,\ 1.0,\ 1.5$; (b) $\Delta = 40,\ \varepsilon = 1.5$; (c) $\Delta = 400,\ \varepsilon = 1.5$; (d)$\Delta = 2000,\ \varepsilon = 1.5$. From left to right in (b)–(d) $N_1/N_2 = 0.05,\ 0.1,\ 0.15,\ 0.25,\ 0.5,\ 0.8,\ 1.2,\ 2.0$.

$S(t) > 0$ while $k(t) < 0$. In other words, barriers disappear before particles passing over x_b. To avoid such phenomenon, it should be guaranteed that $S(t_c) \approx 0$; i.e., $\exp[-\int_0^{t_c} k(\tau)d\tau] \approx 0$. This can be realized by letting $\int_0^{t_c} k(\tau)d\tau > N_2$, where N_2. is a large positive real number. Then it yields

$$F_0 < \frac{N_1}{N_2}\frac{1}{\sqrt{\pi}}\frac{D\Delta^{1.5}}{x_b^3}. \tag{33}$$

When we want to have a high accuracy, we need to choose a rather large N_2, say, $N_2 = 7$, but a relatively moderate N_2, say, $N_2 = 3.0$, is also applicable when high accuracy is not seriously required. So for fixed Δ, a larger D will generate a larger range of effective pulling external forces. From inequality (33), the effectiveness of KA is not only restricted by Δ, but also strongly affected by D. This is why for small D the valid range of F_0 decreases. In Fig. 2, when we set $N_1/N_2 = 0.5$, for $D = 0.05$ the critical external force is around $F_0 \approx 113$, and for $D = 0.005$ it is around $F_0 \approx 11.3$, which coincides with the figures.

In the presence of roughness, to ensure the effectiveness of KA, we restrict F_0 to be small; i.e., N_1/N_2 is small. In Fig. 3(a), the barrier height is set $\Delta = 200$, which shows that the fitting is good for small roughness, while it is bad for large roughness. Due to the important influences of Δ on KA, we discuss here the effectiveness of KA in the rough cases for different Δ. For the convenience of simplicity, the fittings in Figs. 3(b)–3(d) are conducted for $\varepsilon = 1.5$. In Fig. 3(b) when Δ is small, we see that the fitting is not good for either large or small F_0, but when $N_1/N_2 \approx 0.5$, the fitting is rather good. This phenomenon is also found for higher barriers in Figs. 3(c) and 3(d) for $\Delta = 400$ and $\Delta = 2000$; i.e., no matter whether decreasing or increasing F_0, the fitting gets worse in the two extremes. Thus generally, the KA of FPTD for rough potentials is valid for high barriers and moderate external forces only.

B. Validity of PAA

In clear contrast to the Kramers theory, PAA is directly based on a transient evaluation of probability rather than on quasistationary assumptions. Due to the difficulty of obtaining the PDF of a conditionally bounded FPE, this approximation uses a relationship between the FPTD and the natural boundary FPE, from which the FPTD can be precisely derived by an iterationlike procedure as shown in Eq. (26).

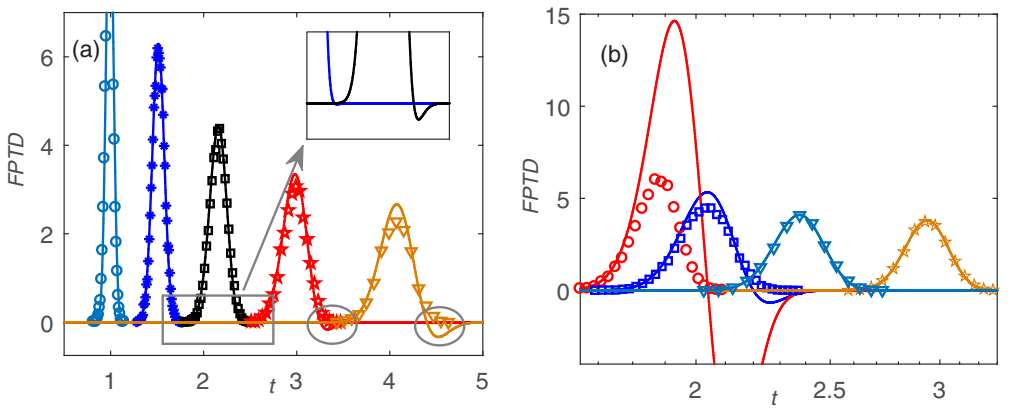

FIG. 4. Comparisons of analytical results without normalization (solid lines) and numerical simulations (symbols) of FPTDs with respect to different parameters in the absence of roughness; $\Delta = 200$. (a) $D = 0.05$, FPTDs for different external forces F_0. From left to right, the solid lines and symbols correspond to $F_0 = 250,\ 150,\ 100,\ 70,\ 50$, and the inset shows the shapes of tails for $F_0 = 150$ and $F_0 = 100$. (b) $F_0 = 100.0$, FPTDs for different D. The solid lines and symbols from left to right correspond to $D = 0.5,\ 0.1,\ 0.025,\ 0.01$.

However, for simplicity, we take the first-order approximation. Figure 4 shows the comparisons of the analytical approximation Eq. (32) and numerical simulations in the absence of roughness.

Being opposite to the KA, in Fig. 4(a), the analytical results have better agreement with numerical results for large F_0, while KA fits better for smaller F_0. But it is similar that the analytical $f(x_b, t)$ may also have negative values at the rhs tail (e.g., $F_0 = 70$ and 50) and it induces nonoverlapping symbols and the solid line near the maximum and rhs tail. Obviously, the negative part greatly influences the validity of the approximation. Besides, in Fig. 4(b) when F_0 is fixed, we find that for larger D this approach breaks down. Therefore to guarantee the validity of the approximation, it is essential to get the effective region of F_0, D, and Δ. For convenience, we denote $f(x_b, t) = Dg(x_b, t)p_n(x_b, t)$, where $g(x_b, t) = -2\Delta/x_b + F_0 t - 2\sigma^{-2}[x_b - \bar{x}(t)]$. In fact, the failure of the approximation is caused by a nonsynchronous variation of $g(x_b, t)$ and $p_n(x_b, t)$. If $g(x_b, t)$ changes from positive to negative at time $\bar{t}_c$ but $p_n(x_b, t) \gg 0$ at the same time, $f(x_b, t)$ will exhibit directly the coexistence of positive and negative parts, and will break down. Thus, it should require $p_n(x_b, \bar{t}_c)$ to be very small or even zero. To process this, firstly, we need to get $\bar{t}_c$. Because $e^{-2Dkt} \to 0$ with time going on, it yields

$$F_0 \bar{t}_c = \frac{2\Delta}{x_b} + \frac{F_0 \Delta}{D x_b^2}. \tag{34}$$

To guarantee $p_n(x_b, \bar{t}_c) \approx 0$, we use the 3σ principle that for a normal distribution $P\{x \notin (\mu - 3\sigma, \mu + 3\sigma)\} \approx 0.3\%$, so we have

$$|x_b - \bar{x}(\bar{t}_c)| > 3\sigma, \tag{35}$$

which leads to

$$F_0 > 6\sqrt{2}\frac{D\Delta^{1.5}}{x_b^3}. \tag{36}$$

In Fig. 4(a), $6\sqrt{2}D\Delta^{1.5}/x_b^3 \approx 150$, the inset figure shows that the rhs tail of $F_0 = 150$ almost disappears, while $F_0 = 100$ has a small negative tail, which coincides with the prediction inequality (36). However, sometimes a small negative part does not seriously break the validity of the analytical approximation, e.g., the shape and the maximum of FPTDs. Therefore we can extend the restriction of the 3σ principle to 2σ if one is not concerned much with highly precise fitting. For the 2σ rule, $F_0 > 4\sqrt{2}D\Delta^{1.5}/x_b^3$. In Fig. 4(b), for fixed $F_0 = 100$, as expected, with the increasing of D the fitting becomes worse and worse. Besides, for larger D it needs less time to pass over x_b.

For KA, smaller F_0 generates better performances, while for PAA the larger the pulling force F_0 the better the fitting. These two methods are complementary to solving the first-passage problem. Next we will check the effectiveness of the analytical approximation for rough potentials.

In the presence of roughness, by spatial averaging we transfer the rough potential problem to a corresponding smooth potential $U^*(x, t)$ and a diffusion coefficient D^*. Figure 5 shows the analytical results of Eq. (32) and the corresponding numerical simulations. In Fig. 5(a), when Δ and F_0 are small, the analytical and the numerical results are almost overlapping even for large roughness $\varepsilon = 1.5$. Besides, we see that with increasing ε, the FPTD moves to the right direction as a whole; i.e., the roughness delays the first-passage process. Besides, the most probable passage time, i.e., the maximum of FPTD, increases with ε. Figures 5(b)–5(d) show the FPTD with respect to $\varepsilon = 0.5,\ 1.0,$ and 1.5, for different Δ. To guarantee the validity of the analytical approximation, the external force is set $F_0 = 4\sqrt{2}D\Delta^{1.5}/x_b^3$. It shows that for a small roughness $\varepsilon = 0.5$ the overlap between the symbols and the solid lines confirms the efficiency of the analytical approximation. For large ε, when Δ is small the agreement is still good. However, when Δ gets larger the fitting becomes worse. In fact, when Δ is large, the rough part $U_1(x) = \varepsilon \cos(\omega x)$ is so small compared to the parabolic potential $U_0(x) = \Delta x^2/x_b^2$ that rough wells almost disappear for large x. At this time, the roughness ε actually affects slightly. Thus under this condition, PAA loses accuracy but remains applicable, but for a low barrier, the analytical approximation is of high efficiency.

Finally, we give the effective regions of both approximations of FPTD for smooth potentials. In region 1 of Fig. 6, one gets a precise PAA of FPTD which corresponds to larger

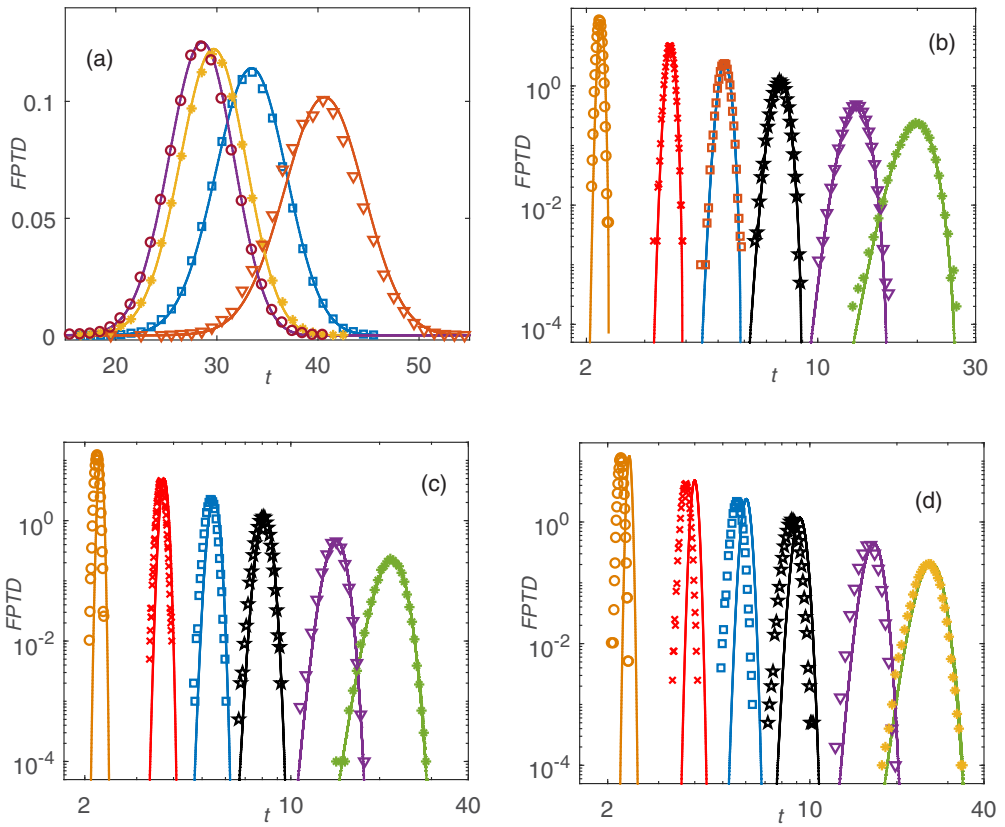

FIG. 5. In the presence of roughness, comparisons of analytical results and numerical simulations of FPTDs with respect to different roughness ε. for $D = 0.01$. (a) $\Delta = 20$, $F_0 = 1.0$ for different roughness from left to right. $\varepsilon = 0,\ 0.5,\ 1.0,\ 1.5$. (b) $\varepsilon = 0.5$. (c) $\varepsilon = 1.0$. (d) $\varepsilon = 1.5$. Panels (b)–(d) are in log-log plots for $\Delta = 2000,\ 800,\ 400,\ 200,\ 80,\ 40$, and $F_0 = 4\sqrt{2}D\Delta^{1.5}/x_b^3$.

external forces, while in region 2, the PAA is also applicable but with small differences in the numerical results. Similarly, for KA of FPTD, region 4 generates a precise fitting and region 3 is valid with loose fitting. In the white area with a gap width $(2\sqrt{2} - \pi^{-0.5})D\Delta^{1.5}/x_b^3$, both approximations are not good enough to fit the FPTD. It is obvious that the effective area of KA is extremely limited by low barriers and small D, while that of PAA is much broader. Thus the two approximations are complementary for FPTD, but there is still a gap between both approximations to be solved.

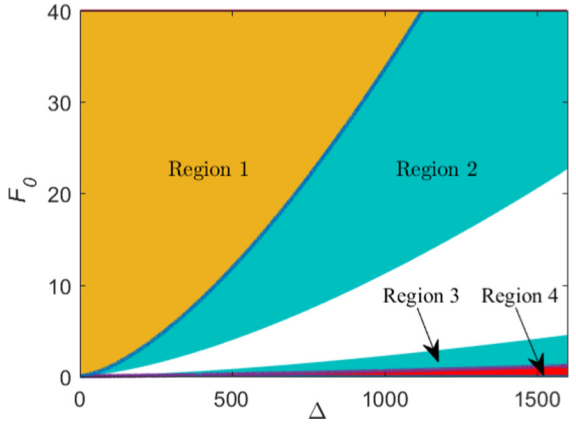

FIG. 6. Illustration of valid areas of KA and PAA of FPTD with $D = 0.01$. Region 1 is separated by the line $F_0 = 6\sqrt{2}D\Delta^{1.5}/x_b^3$. Region 2 and the white area are separateby the line $F_0 = 2\sqrt{2}D\Delta^{1.5}/x_b^3$. The line between region 3 and the white area is $F_0 = \pi^{-0.5}D\Delta^{1.5}/x_b^3$. Region 4 is limited by the line $F_0 = 0.25\pi^{-0.5}D\Delta^{1.5}/x_b^3$.

V. MEAN FIRST-PASSAGE TIME

The probability expectation is an important indicator in experiments because it is easy to conclude and represents the mean level of experimental data. In this part, we try to test the effectiveness of KA and PAA of MFPT, and the influences of roughness on MFPT. To calculate the MFPT, we have to eliminate the inevitable negative value of $f(x_b, t)$ by setting

$$\bar{f}(x_b, t) = \begin{cases} f(x_b, t), & f(x_b, t) > 0 \\ 0, & \text{otherwise} \end{cases}. \tag{37}$$

Thus the MFPT can be obtained by

$$\langle T \rangle = N_3 \int_0^\infty t\bar{f}(x_b, t)dt, \tag{38}$$

where $N_3 = 1/\int \bar{f}(x_b, t)dt$ is the normalized coefficient.

For the KA Eq. (16), when the external force is sufficiently small, i.e., $F \ll D\Delta^{1.5}/x_b^3$, the KA of FPTD exhibits good fitting, i.e. $N_3^K \approx 1.0$. In this case, Garg [43] has given a detailed procedure to get $\langle T \rangle_K$ and the corresponding variance. The MFPT can be approximated as

$$\langle T \rangle_K = \frac{2\Delta}{x_b F} - \frac{2\sqrt{\Delta}}{x_b F}\sqrt{\gamma + \ln\frac{\Delta^{1.5}}{\sqrt{\pi}Fx_b^3}}, \tag{39}$$

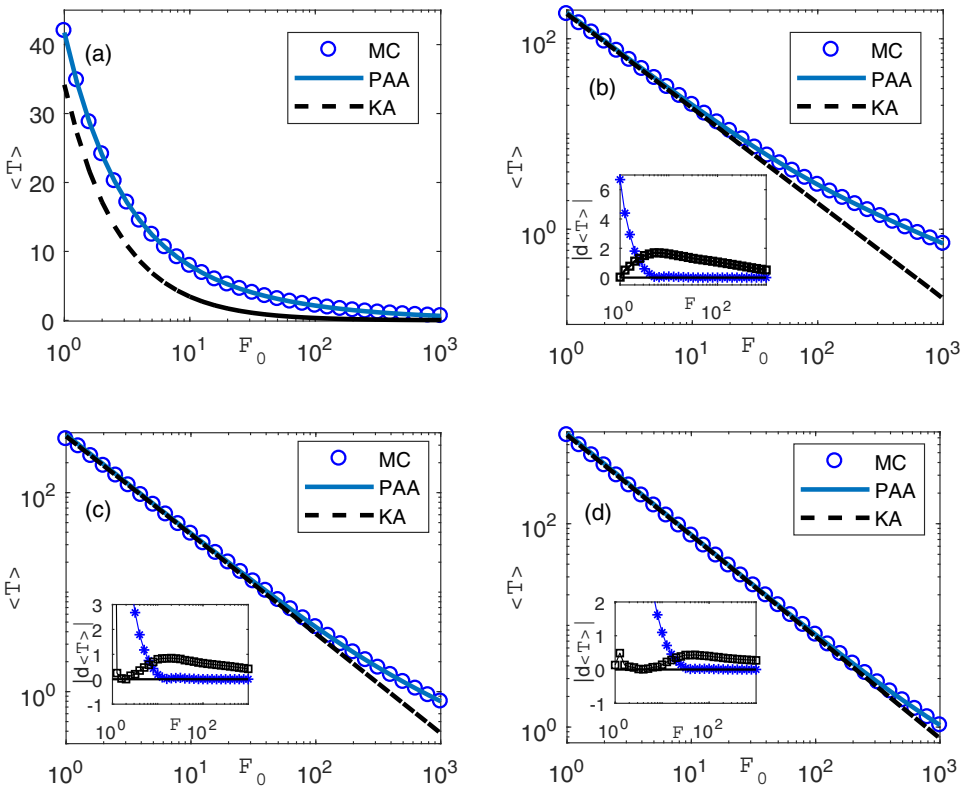

FIG. 7. The MFPTs in the absence of roughness, and the numerical simulations with different F_0 and Δ when $\varepsilon = 0$, $D = 0.01$. The insets are corresponding absolute differences between theoretical results and numerical results, in which blue stars are for PAA and black squares are for KA. The dashed lines are KA of MFPT, the solid lines are PAA of MFPT, and the circles are numerical results. (a) $\Delta = 40$; (b) $\Delta = 200$; (c) $\Delta = 400$; (d) $\Delta = 800$.

in which $\gamma = 0.577$ is the Euler-Mascheroni constant. For intermediate external forces, we directly integrate Eq. (37) with numerical methods.

For PAA [Eq. (32)], when F_0 is relatively small, $e^{-2Dkt} \to 0$ before exiting. We arrive at a result with the form of

$$\langle T\rangle_P = \frac{2}{4D\Delta^{1.5} + \sqrt{\pi}x_b^3 F}\left\{\frac{4D\Delta^{2.5}}{x_b F_0} - x_b^2\sqrt{\Delta} + \left(2x_b^2\Delta + \frac{F_0 x_b^5}{2D\Delta} - \frac{4D\Delta^2}{x_b F_0}\right)\mathrm{erf}(2\Delta)\right\}, \quad (40)$$

where $\mathrm{erf}(x)$ is the error function, and can be approximated by an algebraic formula as $\mathrm{erf}(x)^2 = 1 - \exp(-4x^2/\pi)[1 + 8x^4/\pi(1/3 - 1/\pi)]$. When the external force is sufficiently large, $F_0 \gg D\Delta^{1.5}/x_b^3$, particles will exit quickly. Thus, it is not proper to set e^{-2Dkt} as zero. Due to the complexity of the formula, for large F_0 we derive the MFPT by directly computing Eq. (37).

In Fig. 7, solid lines are the PAA of MFPT, dashed lines are the KA of MFPT, and the circles are numerical results. We find that the PAA is in good agreement with numerical results for the whole range of Δ, and the fitting gets better and

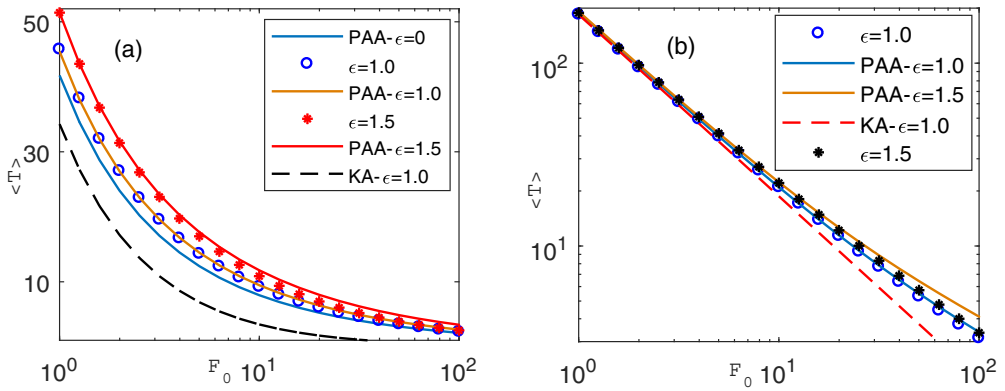

FIG. 8. The MFPTs in rough potentials with different F_0 and ε with $D = 0.05$. (a) $\Delta = 40$; (b) $\Delta = 200$. The solid lines are PAA of MFPT, the dashed lines are KA of MFPT, and the symbols are corresponding numerical results with different ε.

better with increasing F_0, while KA fails on small Δ even with small F_0 in Fig. 7(a). With increasing Δ, the effective region of F_0 for KA becomes larger. The insets in Fig. 7 calculate the absolute differences between analytical approximations and numerical simulation. As shown, the differences between PAA and numerical results decrease with F_0, and tend to zero for large F_0 which indicates the effectiveness of PAA. However, for KA the differences are negligible only for small F_0. Thus, the two methods can be complementary, that is, if one considers sufficiently small F_0, it is better to use KA, otherwise PAA is preferred.

Considering rough potentials, we see that the roughness can increase the MFPT. In Fig. 8(a), it is apparent that PAA is able to fit the numerical results for relatively small F_0, while KA is invalid in the whole range of F_0. For a higher barrier in Fig. 8(b), although KA is close to the numerical results for small F_0, it quickly loses efficacy with increasing F_0, while PAA has a larger effective region of F_0. As shown, both KA and PAA break down when F_0 is large. In fact, for large F_0, the external force F_0 is dominant to make particles exit the boundary, while the effect of diffusion is subordinate. So particles are forced by a large F_0 to pass over the boundary before they have sufficiently long time to diffuse in rough potentials. Thus in our approximation the effective diffusion coefficient is actually meaningless for large F_0. In this case, we suggest to use D instead of D^* even for rough potentials.

VI. CONCLUSION

In this paper, we have provided two approximate methods to obtain analytical solutions of the first-passage-time distribution and the mean first-passage time in a moving parabolic potential for the cases with and without roughness. In the absence of a rough potential, we have obtained the KA of FPTD. However, due to the assumptions of high barriers and quasistationarity, KA fails for large external forces and small diffusion coefficient. It should generally follow the relationship of $F_0 \ll D\Delta^{1.5}/x_b^3$ to guarantee the validity of KA both for FPTD and MFPT. We have found that compared to the FPTD, the MFPT has a larger effective region of external forces. This is because although the KA of FPTD fits badly, its peak does not differ much from the numerical results, which makes MFPT valid for a relatively larger external force. To overcome the shortage of KA, we have referred to Giorno's equation and approximate the FPTD based on the PDF obtaining from the FPE with a natural boundary rather than an absorbing boundary. Being opposite to KA, the PAA is highly effective even for large external forces obeying the relationship $F_0 \gg D\Delta^{1.5}/x_b^3$. However, although the PAA of FPTD is not so ideal for small external forces, it shows that the MFPT in small external force cases can also well fit the numerical simulation. Thus, the PAA of MFPT is valid for almost the whole range of external forces.

In the presence of a rough potential, we have used spatial averaging approximation to smooth the rough potential, and obtain an effective smooth potential and a diffusion coefficient. By combining these effective factors and analytical results for smooth potentials, the corresponding KA and PAA of FPTD and MFPT in the rough case are obtained. It shows that in rough potentials KA of FPTD fits well for moderate external forces and the fitting becomes better with increasing the barriers. On the contrary, the PAA of FPTD is in better agreement with numerical simulations for a low barrier. With increasing the roughness, the fitting becomes worse, and it is even worse for higher barriers. However, the PAA of MPFT is valid on the whole ranges of barriers and external force, which indicates that although PAA of FPTD loses accuracy, it differs slightly from the exact results. Besides, the superposition of the rough potential will shift the FPTD to the right. Thus, the roughness leads to longer time for particles to pass over the boundary.

ACKNOWLEDGMENTS

This work was supported by the China Postdoctoral Science Foundation funded project, the NSF of China (Grant No. 11772255), the Fundamental Research Funds for the Central Universities, and Shaanxi Project for Distinguished Young Scholars. We also thank Prof. Jinqiao Duan for helpful discussions.

APPENDIX

Here we explain how to derive the approximations of rates k_0 and $k_F(t)$. Firstly, for a simple parabolic potential $U_0(x) = \frac{\Delta}{x_b^2}x^2$, the integral over the potential well $\int_{\text{well}} e^{-U_0(y)}dy$ can be approximated as follows.

$$\frac{1}{2}\sqrt{\frac{\pi}{\Delta}}x_b = \int_{-\infty}^{0} e^{-\frac{\Delta}{x_b^2}x^2}dx \leqslant \int_{\text{well}} e^{-\frac{\Delta}{x_b^2}x^2}dx \leqslant \int_{-\infty}^{+\infty} e^{-\frac{\Delta}{x_b^2}x^2}dx = \sqrt{\frac{\pi}{\Delta}}x_b. \tag{A1}$$

For the integral $\int_{\text{b}} e^{U_0(y)}dy$, we can get its value interval as

$$\int_{\text{b}} e^{\frac{\Delta}{x_b^2}x^2}dx = e^{\Delta}\int_0^{x_b} e^{\frac{\Delta}{x_b^2}(x^2-x_b^2)}dx \leqslant e^{\Delta}\int_0^{x_b} e^{\frac{\Delta}{x_b^2}[2x_b(x-x_b)]}dx = x_b\Delta^{-1}e^{\Delta}(1-e^{-\Delta}), \tag{A2}$$

and

$$\int_{\text{b}} e^{\frac{\Delta}{x_b^2}x^2}dx = e^{\Delta}\int_0^{x_b} e^{\frac{\Delta}{x_b^2}(x^2-x_b^2)}dx \geqslant e^{\Delta}\int_0^{x_b} e^{\frac{\Delta}{x_b^2}[x_b(x-x_b)]}dx = \frac{1}{2}x_b\Delta^{-1}e^{\Delta}(1-e^{-\Delta}). \tag{A3}$$

Combining Eqs. (A1)–(A3) yields

$$\frac{1}{4}\sqrt{\pi}x_b^2\Delta^{-1.5}e^{\Delta}(1-e^{-\Delta}) \leqslant Dk_0^{-1} \leqslant \sqrt{\pi}x_b^2\Delta^{-1.5}e^{\Delta}(1-e^{-\Delta}). \tag{A4}$$

When $\Delta \gg 1$, we can get the escape rate

$$D\frac{\Delta^{1.5}}{\sqrt{\pi}x_b^2}e^{-\Delta} \leqslant k_0 \leqslant 4D\frac{\Delta^{1.5}}{\sqrt{\pi}x_b^2}e^{-\Delta}. \tag{A5}$$

Thus $k_0 = N_1 D\frac{\Delta^{1.5}}{\sqrt{\pi}x_b^2}e^{-\Delta}$. For time-dependent potentials,

$$U_0(x) + F(x,t) = \frac{\Delta}{x_b^2}x^2 - F_0 xt = \frac{\Delta}{x_b^2}\left(x - \frac{x_b^2}{2\Delta}F_0 t\right)^2 - \frac{x_b^4}{4\Delta}F_0^2 t^2. \tag{A6}$$

Substituting Eq. (A6) to Eqs. (A1)–(A4), and repeating the process, one can get the approximation of $k_F(t)$ as

$$k_F(t) = N_1 D\frac{\Delta^{1.5}}{x_b^2\sqrt{\pi}}[1 - x_b F_0 t/2\Delta]e^{-\Delta(1-x_b F_0 t/2\Delta)^2}. \tag{A7}$$

[1] W. Horsthemke and R. Lefever, *Noise-induced Transitions* (Springer, Berlin, 2006).
[2] R. Lua and A. Grosberg, Phys. Rev. E **72**, 061918 (2005).
[3] T. Spanio, J. Hidalgo, and M. Muñoz, Phys. Rev. E **96**, 042301 (2017).
[4] Z. Q. Wang, Y. Xu, and H. Yang, Sci. China Technol. Sci. **59**, 371 (2016).
[5] S. Dev and S. Chatterjee, Phys. Rev. E **91**, 042714 (2015).
[6] A. Godec and R. Metzler, Phys. Rev. X **6**, 041037 (2016).
[7] A. Godec and R. Metzler, Sci. Rep. **6**, 20349 (2016).
[8] Y. Xu, J. Feng, J. H. Li, and H. Q. Zhang, Chaos **23**, 013110 (2013).
[9] H. Risken, *The Fokker-Planck Equation* (Springer, Berlin, 1989).
[10] S. Redner, *A Guide to First-passage Processes* (Cambridge University Press, New York, 2001).
[11] Y. Xu, H. Li, H. Y. Wang, W. T. Jia, X. L. Yue, and J. Kurths, J. Appl. Mech. **84**, 091004 (2017).
[12] M. Nyberg, T. Ambjörnsson, and L. Lizana, New J. Phys. **18**, 063019 (2016).
[13] Z. H. Hu, L. W. Cheng, and B. J. Berne, J. Chem. Phys. **133**, 034105 (2010).
[14] P. Hänggi, P. Talkner, and M. Borkovec, Rev. Mod. Phys. **62**, 251 (1990).
[15] V. I. Mel'nikov, Phys. Rep. **209**, 1 (1991).
[16] O. K. Dudko, G. Hummer, and A. Szabo, Phys. Rev. Lett. **96**, 108101 (2006).
[17] G. Hummer and A. Szabo, Biophys. J. **85**, 5 (2003).
[18] O. K. Dudko, A. E. Filippov, J. Klafter, and M. Urbakh, Proc. Natl. Acad. Sci. USA **100**, 11378 (2003).
[19] L.B. Freund, Proc. Natl. Acad. Sci. USA **106**, 8818 (2009).
[20] C. Gergely, J.-C. Voegel, P. Schaaf, B. Senger, M. Maaloum, J. K. H. Hörber, and J. Hemmerlé, Proc. Natl. Acad. Sci. USA **97**, 10802 (2000).
[21] C. Bucher, A. Di Matteo, M. Di Paola, and A. Pirrotta, Nonlinear Dyn. **85**, 1445 (2016).
[22] I. Kougioumtzoglou and D. Spanos, J. Eng. Mech. **139**, 1207 (2013).
[23] J. Bullerjahn, S. Sturm, and K. Kroy, Nat. Commun. **5**, 4463 (2014).
[24] A. Buonocore, A. G. Nobile, and L. M. Ricciardi, Adv. Appl. Probab. **19**, 784 (1987).
[25] V. Giorno, A. G. Nobile, L. M. Ricciardi, and S. Sato, Adv. Appl. Probab. **21**, 20 (1989).
[26] I. Pavlyukevich, B. Dybiec, A. Chechkin, and I. M. Sokolov, Eur. Phys. J. Special Topics **191**, 223 (2010).
[27] I. Pavlyukevich, Stochastic Dyn. **11**, 495 (2011).
[28] C. Hyeon and D. Thirumalai, Proc. Natl. Acad. Sci. USA **100**, 10249 (2003).
[29] R. Nevo, V. Brumfeld, R. Kapon, P. Hinterdorfer, and Z. Reich, EMBO Rep. **6**, 482 (2005).
[30] L. Delemotte, M. Kasimova, M. Klein, M. Tarek, and V. Carnevale, Proc. Natl. Acad. Sci. USA **112**, 124 (2015).
[31] T. Linder, B. L. de Groot, and A. Stary-Weinzinger, PLoS Comput. Biol. **9**, e1003058 (2013).
[32] P. Charbonneau, J. Kurchan, G. Parisi, P. Urbani, and F. Zamponi, Nat. Commun. **5**, 3725 (2014).
[33] J. C. Ye, J. Lu, C. T. Liu, Q. Wang, and Y. Yang, Nat. Mater. **9**, 619 (2010).
[34] A. Heuer, B. Doliwa, and A. Saksaengwijit, Phys. Rev. E **72**, 021503 (2005).
[35] P. G. Debenedetti and F. H. Stillinger, Nature **410**, 259 (2001).
[36] R. Zwanzig, Proc. Natl. Acad. Sci. USA **85**, 2029 (1988).
[37] E. Pollak, A. Auerbach, and P. Talkner, Biophys. J. **95**, 4258 (2008).
[38] A. Ansari, J. Chem. Phys. **112**, 2516 (2000).
[39] D. Mondal, P. K. Ghosh, and D. S. Ray, J. Chem. Phys. **130**, 074703 (2009).
[40] Y. G. Li, Y. Xu, J. Kurths, and X. L. Yue, Phys. Rev. E **94**, 042222 (2016).
[41] Y. G. Li, Y. Xu, and J. Kurths, Phys. Rev. E **96**, 052121 (2017).
[42] Y. G. Li, Y. Xu, J. Kurths, and X. L. Yue, Chaos **27**, 103102 (2017).
[43] A. Garg, Phys. Rev. B **51**, 15592 (1995).